ICCFD13-2026-191

A Preconditioned Five-Equation Two-Phase Model for Slug Capturing in Inclined and Vertical Pipes

F. Nikfarjam*, H. Anbarlooei* and D. O. A. Cruz**
Corresponding author: farhad.nikfarjam@matematica.ufrj.br
* Department of Applied Mathematics, Federal University of Rio de Janeiro, Brazil.
** Mechanical Engineering Program (COPPE), Federal University of Rio de Janeiro, Brazil.

Abstract: Slug flow is a common flow regime encountered in pipelines and risers used in offshore oil and gas production and transportation systems. In many practical applications within the oil, gas, and process industries, the liquid phase exhibits non-Newtonian behavior. The numerical simulation of such flows often requires the consideration of very long pipelines and long physical integration times, making computational efficiency a major challenge. In this work, a one-dimensional transient slug-capturing framework based on an always-hyperbolic five-equation two-fluid model is developed for the simulation of gas-liquid flows in horizontal, inclined, and vertical pipes. The proposed formulation remains well-posed over the entire range of pipe inclinations and avoids the stability deficiencies commonly encountered in conventional four-equation two-fluid models. To reduce the excessive numerical diffusion associated with the five-equation formulation, a low-Mach-number preconditioning technique is introduced. Through a stability analysis of the complete operator-splitting scheme, it is shown that, contrary to the conventional expectation, the preconditioning procedure does not impose the severe time-step restriction typically associated with low-Mach-number preconditioning. To enable the application of the proposed methodology to industrial-scale problems, the numerical solver is fully implemented on graphics processing units (GPUs), allowing efficient and time-accurate simulations of transient flows in very long pipelines over extended periods of physical time. The predictive capability of the framework is assessed through comparisons with experimental measurements, numerical results, and empirical correlations available in the literature. The results demonstrate that the proposed approach provides an accurate, stable, and computationally efficient tool for the simulation of transient gas-liquid flows in industrial pipeline systems.

Keywords: Two-phase flow, Slug capturing, Low-Mach number preconditioning, Stability Condition, GPU computing.

1. Introduction

Slug flow is a commonly encountered intermittent flow regime in gas-liquid pipelines and risers used in offshore oil and gas production systems. It is characterized by the periodic formation of liquid slugs separated by elongated gas bubbles, leading to strong pressure oscillations and large fluctuations in phase velocities. These features can significantly affect operational safety, flow assurance, and structural integrity of pipeline systems. As a result, accurate prediction of slug flow characteristics has been the subject of extensive experimental and numerical research over the past decades [1, 2].

Pipe inclination plays a critical role in slug initiation, growth, and propagation due to the strong interaction between gravity, phase distribution, and interfacial dynamics. Highly inclined and vertical configurations are particularly challenging because small changes in liquid holdup can substantially alter the flow structure and pressure response. In addition, many industrial applications involve liquids that exhibit non-Newtonian rheological behavior. Shear-thinning fluids are frequently encountered in drilling and completion operations, hydraulic fracturing, slurry transport, and polymer-enhanced hydrocarbon transportation [3, 4, 5]. Such rheological effects can significantly modify wall and interfacial shear stresses, phase distribution, and slug characteristics. Consequently, the development of numerical models capable of accurately describing slug flows in inclined and vertical pipes while accommodating non-Newtonian liquid behavior remains an important challenge.

One-dimensional slug-capturing methods based on two-fluid models have become a standard tool for simulating transient multiphase flows in pipelines, owing to their ability to represent flow-regime transitions and intermittent behavior. These methods can predict stratified and slug flow regimes, as well as transitions between them, while relying on a relatively limited set of empirical closure relations [6]. They are therefore well suited for the simulation of transient operating conditions such as pipeline start-up, shutdown, depressurization, terrain-induced slugging, and severe slugging.

However, the conventional four-equation two-fluid formulation is known to suffer from loss of hyperbolicity under a wide range of practical flow conditions. This ill-posedness may lead to numerical instabilities, non-physical wave propagation, and strong sensitivity to grid resolution and numerical parameters. To illustrate these shortcomings, Fig. 1a presents the solution of a typical horizontal slug-flow problem. In this test case, all inlet and outlet boundary conditions are kept constant in time. Therefore, after a sufficiently long integration period, the solution is expected to reach a statistically developed regime in which the main slug characteristics, such as slug frequency, slug length, and propagation velocity, remain approximately constant. As evident, the four-equation model fails to reproduce the expected statistically developed slug regime. Instead, it generates a dense field of irregular waves, which are often mistakenly interpreted as a physical distribution of slug lengths. Although various numerical regularization techniques have been proposed to alleviate these issues [7], they generally extend the domain of well-posedness rather than guaranteeing unconditional hyperbolicity. Consequently, numerical solutions may remain sensitive to discretization choices and may still exhibit non-physical behavior.

An alternative approach is provided by the five-equation two-fluid formulation, in which an additional volume-fraction transport equation is introduced together with a pressure relaxation mechanism [8, 9]. When combined with an appropriate equation of state, this formulation remains unconditionally hyperbolic and admits a complete set of real eigenvalues for all admissible flow states. The theoretical foundation of this approach originates from multiphase flow models developed for compressible media and has been shown to significantly improve robustness and stability [8, 9].

However, when discretized using upwind finite-volume schemes, the five-equation model is known to suffer from excessive numerical dissipation, particularly in low–Mach-number regimes, which are typical of two-phase pipeline flows [10]. Figure 1b presents the solution obtained for the same slug-flow problem described above. In contrast to the four-equation model, no spurious waves are generated. Nevertheless, numerical diffusion progressively damps the slug structures, eventually causing the flow to evolve toward a stratified configuration. This limitation becomes particularly severe in simulations of long pipelines over extended periods, often on the order of several days, as required in industrial applications. Under such conditions, the excessive numerical dissipation may completely suppress the slug dynamics, rendering the model unsuitable for practical slug-flow predictions.

This issue is closely related to the classical low-Mach-number problem of upwind schemes, such as Roe's method, which lose accuracy and efficiency [11, 12]. In this work, this difficulty is addressed using the well-known preconditioning technique proposed by Turkel [12], which has previously been extended to two-fluid models [13]. The details of the preconditioning strategy are presented in the following sections. Nevertheless, it is instructive to examine its effect on the horizontal slug-flow problem introduced above. Figure 1c shows the solution obtained using the preconditioned five-equation model. In contrast to the previous cases, the preconditioned formulation successfully preserves the slug structures while avoiding the spurious waves observed in the four-equation model. After a sufficiently long integration time, the flow develops a repeatable slugging regime characterized by statistically similar slugs with nearly constant frequency, length, and propagation velocity. Once established, this regime persists throughout the remainder of the simulation. Although preconditioning effectively mitigates numerical dissipation, it is also known to severely deteriorate the CFL stability condition [14, 15, 16]. The resulting time-step

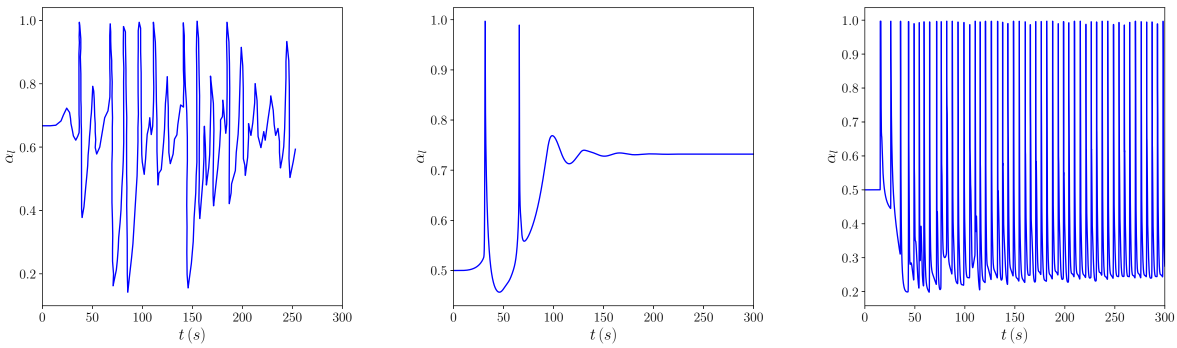

(a) ROE 4 (b) ROE 5 (c) ROE 5 + Preconditioning

Figure 1: Overall Comparison of the Roe scheme applied to the four-equation and five-equation two-fluid models, with and without preconditioning, for a typical horizontal slug-flow problem.

restriction is governed by the local Mach number, often reducing the allowable CFL number from values of order unity to values as small as 10^{-3}. For the long integration times typically required in industrial pipeline simulations, which may span several days of physical time, this additional computational cost becomes prohibitive, thereby limiting the practical applicability of the method.

The main contribution of the present work is to demonstrate that the specific numerical methodology proposed for the solution of the preconditioned five-equation model can substantially alleviate this limitation and recover the stability limits typically associated with the non-preconditioned formulation. To summarize, this work presents a solution methodology for the always-hyperbolic five-equation two-fluid model. The proposed approach is shown to be numerically stable while introducing only minimal numerical diffusion, thereby enabling accurate simulations over very long integration times. Furthermore, it is demonstrated that the stability limits of the method are not adversely affected by the proposed numerical treatment, particularly by the preconditioning of the diffusive terms. Finally, the developed methodology is validated over a broad range of applications, including horizontal and inclined pipe flows as well as non-Newtonian two-phase flows.

2. Numerical Methods

The gas-liquid flow is modeled using a one-dimensional five-equation two-fluid formulation [17, 6]. The governing equations consist of one volume-fraction transport equation, two mass conservation equations, and two momentum equations, written as:

$$
\begin{aligned}
&\frac{\partial \alpha_g}{\partial t} + u_i \frac{\partial \alpha_g}{\partial x} = r_p (p_g - p_l),\\
&\frac{\partial (\alpha_k \rho_k)}{\partial t} + \frac{\partial (\alpha_k \rho_k u_k)}{\partial x} = 0,\\
&\frac{\partial (\alpha_k \rho_k u_k)}{\partial t} + \frac{\partial (\alpha_k \rho_k u_k^2 + \alpha_k p_k)}{\partial x} - p_k^i \frac{\partial \alpha_k}{\partial x} = S_k,
\end{aligned}
\tag{1}
$$

where α_k, ρ_k, u_k, and p_k stand for the volume fraction, density, velocity and pressure of the phase k, respectively. The $k = g, l$ denotes the gas and liquid phases. r_p is the pressure relaxation coefficient and S_k represents the source term which encapsulates the physical effects such as friction and gravity. The limit $r_p \longrightarrow \infty$ corresponds to instantaneous pressure relaxation, yielding mechanical equilibrium between the phases, i.e., $p_g = p_l$ [9]. However, the present formulation does not restrict the analysis to this limiting case and only assumes that the pressure relaxation process is sufficiently fast.

An interface pressure (p_k^i) and an equation of state in the form of $p_k = P_k(\rho_k)$ must be provided for each phase as closure equations. In this work we use Stiffened Gas (SG) equation of state (EOS),

$$p_k = p_{0,k} + c_k^2(\rho_k - \rho_{0,k}), \tag{2}$$

where $p_{0,k}$, $\rho_{0,k}$ and c_k are the reference pressure, the reference density and the speed of sound in each phase, respectively.

The governing equations (1) can be written as:

$$\partial_t \mathbf{q} + \mathbf{A}\ \partial_x \mathbf{q} = \mathbf{R} + \mathbf{S}, \tag{3}$$

where:

$$\mathbf{q} = \begin{bmatrix} \alpha_g \\ \alpha_g\rho_g \\ \alpha_g\rho_g u_g \\ \alpha_l\rho_l \\ \alpha_l\rho_l u_l \end{bmatrix}, \quad \mathbf{A} = \begin{bmatrix} u_i & 0 & 0 & 0 & 0 \\ 0 & 0 & 1 & 0 & 0 \\ -\hat{p}_g & c_g^2 - u_g^2 & 2u_g & 0 & 0 \\ 0 & 0 & 0 & 0 & 1 \\ \hat{p}_l & 0 & 0 & c_l^2 - u_l^2 & 2u_l \end{bmatrix}, \quad \mathbf{R} = \begin{bmatrix} r_p(p_g - p_l) \\ 0 \\ 0 \\ 0 \\ 0 \end{bmatrix}, \quad \mathbf{S} = \begin{bmatrix} 0 \\ 0 \\ S_g \\ 0 \\ S_l \end{bmatrix}. \tag{4}$$

Here to simplify the equations, we defined $\hat{p}_k = p_k^i - p_{0,k} + c_k^2\rho_{0,k}$.

We are interested in flows where $u_k \ll c_k$. Therefore, the system (3) is unconditionally hyperbolic and always has five distinct eigenvalues:

$$\lambda = [u_i, u_g - c_g, u_g + c_g, u_l - c_l, u_l + c_l]^T. \tag{5}$$

Using the fractional splitting method [9, 18, 19], the system (3) could be split into three sub-problems that can be solved independently at each time step. The first part, the homogeneous partial differential equations, hereinafter called the hyperbolic step and reads as:

$$\frac{\partial \mathbf{q}}{\partial t} + \mathbf{A}\frac{\partial \mathbf{q}}{\partial x} = 0. \tag{6}$$

After solving one step of the hyperbolic part, one needs to apply the effect of the source and relaxation terms which are two simple ordinary differential equations:

$$\frac{d\mathbf{q}}{dt} = \mathbf{S}(\mathbf{q}) \quad , \quad \frac{d\mathbf{q}}{dt} = \mathbf{R}(\mathbf{q}). \tag{7}$$

Based on fractional splitting, the solution is advanced according to

$$q^* = \mathcal{L}_H(q^n) \quad \rightarrow \quad q^{**} = \mathcal{L}_R(q^*) \quad \rightarrow \quad q^{n+1} = \mathcal{L}_S(q^{**}),$$

where $\mathcal{L}_H$, $\mathcal{L}_R$ and $\mathcal{L}_S$ denote the hyperbolic, relaxation, and source-term operators, respectively. In the following sections, the individual operators are described in detail. We first present the source-term operator, followed by the pressure-relaxation operator, and finally the hyperbolic operator.

2.1 Source terms

In the present work, only the momentum source terms associated with gravity and wall friction are considered, while mass transfer between the phases is neglected. The corresponding source terms can be written as:

$$\begin{aligned} S_g &= -\alpha_g\, \rho_g\, g\, sin(\theta) - F_g^w - F_i, \\ S_l &= -\alpha_l\, \rho_l\, g\, sin(\theta) - F_l^w + F_i. \end{aligned} \tag{8}$$

Here, g and θ are the acceleration due to gravity and the inclination angle of the pipe. The wall frictional forces for each phase is defined as $F_{kw} = \tau_{kw} S_k/A$, and the interfacial force between gas and the liquid phases is defined as $F_i = \tau_i S_i/A$, where A, S_k and S_i are the area of the pipe, the wetted perimeter by each phase and the interfacial surface between phases, respectively. The shear stresses on the pipe wall for each phase then is obtained using $\tau_{kw} = \frac{1}{2} f_k \rho_k u_k^2$ and between phases as $\tau_i = \frac{1}{2} f_i \rho_g (u_g - u_l)^2$.

In the present work, the closure models have been extended to handle the purely viscous non-Newtonian liquid phase based on the friction factor equations developed in [20, 21]. For the simplest case of the power-law type fluid, the laminar friction factor is $f = 16/Re_{\text{MR}}$, where the Metzner-Reed Reynolds number is defined as:

$$Re_{\text{MR}} = \frac{\rho U^{2-n} D^n}{K 8^{n-1} (\frac{3n+1}{4n})^n}.$$

Based on the theory developed in [20, 21], the turbulent friction factor is given by:

$$f = C_f \, Re_{\text{G}}^{-\frac{1}{2n+2}}, \tag{9}$$

where C_f is the proportionality constant which assumed to be equal to the Blasius constant (0.079). The generalized Reynolds number in this equation is defined as $Re_{\text{G}} = \rho \, U^{2-n} \, D^n / K$. The transition Reynolds number (from laminar flow to turbulent flow) is modeled using the correlation suggested in [22], as $Re_{\text{MR}}^{\text{trans}} = 3250 - 1150 \, n$, where n is the flow exponent of the power-law model.

Finally, the source-term operator is integrated in time using the explicit forward Euler method.

2.2 Relaxation Step

Based on the fractional splitting introduced above, the relaxation equations can be written as:

$$\frac{\partial \alpha_g}{\partial t} = r_p \, (p_g - p_l), \tag{10}$$

$$\frac{\partial (\alpha_k \rho_k)}{\partial t} = 0, \tag{11}$$

$$\frac{\partial (\alpha_k \rho_k u_k)}{\partial t} = 0. \tag{12}$$

It is evident that $\alpha_k \, \rho_k$ and $\alpha_k \, \rho_k \, u_k$ terms remain constant during the relaxation step.

In the limit $r_p \longrightarrow \infty$, the first equation reduces to the mechanical equilibrium condition $p_g = p_l = p$ [9]. Then using $\alpha_g + \alpha_l = 1$ and the fact that $\rho_k(p)$, one has:

$$\alpha_g + \alpha_l = \frac{(\alpha_g \rho_g)^*}{\rho_g(p)} + \frac{(\alpha_l \rho_l)^*}{\rho_l(p)} = 1. \tag{13}$$

Assuming the SG equation of state, Eq. (13) can be reduced to a quadratic equation, for which only one root is physically admissible:

$$p^{**} = \frac{-\xi_1 + \sqrt{\xi_1^2 - 4\xi_2}}{2}, \tag{14}$$

where $\xi_1 = A_g + A_l - c_g^2 (\alpha_g \rho_g)^* - c_l^2 (\alpha_l \rho_l)^*$ and $\xi_2 = A_g A_l - A_g c_l^2 (\alpha_l \rho_l)^* - A_l c_g^2 (\alpha_g \rho_g)^*$. Ak is also defined as $\rho_{0,k} c_k^2 - P_{0,k}$. Then using $\alpha_g^{**} = (\alpha_g \rho_g)^* / \rho_g(p^{**})$, one can calculate the relaxed volume fraction. At this stage, the state vector becomes $q^{**} = [\alpha_g^{**}, \alpha_k^* \rho_k^*, \alpha_k^* \rho_k^* u_k^*]^T$.

It is worth noting that, if finite-rate relaxation is assumed, Eq. (10) becomes:

$$\frac{d\alpha_g}{dt} = r_p \left(p_g \left(\frac{\alpha_g^* \rho_g^*}{\alpha_g} \right) - p_l \left(\frac{\alpha_l^* \rho_l^*}{1 - \alpha_g} \right) \right), \tag{15}$$

which results in a nonlinear ordinary differential equation for α_g.

2.3 Hyperbolic Step

To solve the hyperbolic part of the system, a finite-volume discretization combined with a Roe-type linearization is employed. The resulting discrete equations can then be written as:

$$\mathbf{Q}_{h,i}^{n+1} = \mathbf{Q}_i^n - \frac{\Delta t}{\Delta x}\left(\mathbf{A}^+_{i-1/2}\Delta\mathbf{Q}_{i-1/2} + \mathbf{A}^-_{i+1/2}\Delta\mathbf{Q}_{i+1/2}\right), \tag{16}$$

where $\mathbf{Q}_i$ represents the volume averaged $\mathbf{q}$, calculated at the cell centers of a collocated grid in finite volume discretization [18, 19, 17]. Vectors $\mathbf{A}^{\pm}\Delta\mathbf{Q}$ are fluctuations arising from the Riemann problems at the cell interfaces $x_{i\pm 1/2}$, obtained by solving Eq. (3) [18, 19]. Since $\mathbf{A}$ is always diagonalizable, the fluctuation terms appearing in Eq. (16) can be decomposed as:

$$\mathbf{A}^{\pm}\Delta\mathbf{Q} = \mathbf{R}\mathbf{\Lambda}^{\pm}\mathbf{R}^{-1}\Delta\mathbf{Q} \tag{17}$$

where $\mathbf{R}$ is the matrix of eigenvectors of $\mathbf{A}$, $\mathbf{\Lambda}^{\pm} = \text{diagonal}(\lambda_j^{\pm})$ is a diagonal matrix with the diagonal elements defined as $\lambda_j^{\pm} = \frac{1}{2}\left(\lambda_j \pm |\lambda_j|\right)$, and λ_j stands for the eigenvalues of $\mathbf{A}$. To separate the numerical viscosity contribution, Eq. (16) can be rearranged as [13]:

$$\mathbf{Q}_{h,i}^{n+1} = \mathbf{Q}_i^n - \frac{\Delta t}{\Delta x}\left(\mathbf{A}_{i+1/2}\Delta\mathbf{Q}_{i+1/2} + \mathbf{A}_{i-1/2}\Delta\mathbf{Q}_{i-1/2}\right) + \frac{\Delta t}{\Delta x}\left(|\mathbf{A}|_{i+1/2}\Delta\mathbf{Q}_{i+1/2} - |\mathbf{A}|_{i-1/2}\Delta\mathbf{Q}_{i-1/2}\right), \tag{18}$$

where the last term in RHS is responsible for the numerical diffusion. As discussed previously, this method exhibits excessive numerical diffusion and is therefore unsuitable for the very long integration times considered in the present work. The preconditioning technique, which is introduced in the next section, effectively controls and limits this numerical diffusion, thereby overcoming this limitation. It should be noted that the preconditioning procedure affects only the diffusive terms in Eq. (18) in the low-Mach-number regime. Additional details regarding the preconditioning strategy are provided in section 3.

3. Preconditioning

In the present work, the Turkel preconditioning technique [12, 23, 13] is employed in conjunction with Roe's method. This approach regulates the numerical dissipation in the low-Mach-number limit and is extended here to the five-equation system given by Eq. (16). In this method, the viscous dissipation $|\mathbf{A}|\Delta\mathbf{Q}$ in (18) is replaced with:

$$\mathcal{V}^P\Delta\mathbf{Q} = \mathbf{P}^{-1}|\mathbf{P}\,\mathbf{A}|\Delta\mathbf{Q}, \tag{19}$$

where $\mathbf{P}$ is the preconditioning matrix and $\mathcal{V}^P$ is the preconditioned numerical diffusion. By analogy with Turkel's preconditioning matrix for single-phase flows, we propose the following preconditioning matrix::

$$\mathbf{P}^{\phi} = \begin{bmatrix} \beta_g^2 & 0 & 0 & 0 & 0 \\ 0 & \beta_l^2 & 0 & 0 & 0 \\ 0 & 0 & 1 & 0 & 0 \\ 0 & 0 & 0 & 1 & 0 \\ 0 & 0 & 0 & 0 & 1 \end{bmatrix} \tag{20}$$

with the basis of $\phi = [p_g, p_l, u_g, u_l, \alpha_g]^T$. The parameter β_k is proportional to the local Mach number $M_k = u_k/c_k$ when $M_k < 1$ and $\beta_k = 1$ otherwise. The preconditioning matrix in the conservative variables space ($[\alpha_g, \alpha_k\rho_k, \alpha_k\rho_k u_k]$) then becomes:

$$\mathbf{P}(\mathbf{q}) = \frac{\partial \mathbf{q}}{\partial \phi}\mathbf{P}^{\phi}\frac{\partial \phi}{\partial \mathbf{q}} = \begin{bmatrix} 1 & 0 & 0 & 0 & 0 \\ \rho_g(1-\beta_g^2) & \beta_g^2 & 0 & 0 & 0 \\ \rho_g u_g(1-\beta_g^2) & u_g(\beta_g^2-1) & 1 & 0 & 0 \\ \rho_l(\beta_l^2-1) & 0 & 0 & \beta_l^2 & 0 \\ \rho_l u_l(\beta_l^2-1) & 0 & 0 & u_l(\beta_l^2-1) & 1 \end{bmatrix}. \tag{21}$$

The eigenvalues of the matrix $\mathbf{P}\,\mathbf{A}$ become:

$$\lambda^P = \left[u_i, \frac{1}{2}\left((\beta_g^2+1)\,u_g \pm \sqrt{\Delta_g}\right), \frac{1}{2}\left((\beta_l^2+1)\,u_l \pm \sqrt{\Delta_l}\right)\right]^T, \tag{22}$$

where:

$$\Delta_g = [(\beta_g^2-1)\,u_g]^2 + 4\beta_g^2 c_g^2 \quad ; \quad \Delta_l = [(\beta_l^2-1)\,u_l]^2 + 4\beta_l^2 c_l^2. \tag{23}$$

Comparing eigenvalues of the preconditioned matrix in (22) with the eigenvalues of the matrix $\mathbf{A}$ (5) shows that preconditioning is equivalent to use an effective wave speed which is lower than the actual sound speed. Munkejord [17] observed that lowering the liquid sound speed reduces the undesirable smearing of the ROE-5 solver. As evident from Eq. (22), decreasing β_k is equivalent to lowering the effective sound speed of the phase k, which fulfills this.

The preconditioning parameter is usually selected as:

$$\beta_k^2 = min\left(max\left(\epsilon, k_1 M_k^2\right), 1\right), \tag{24}$$

where the constant k_1 depends on the problem. The cutting parameter is defined as $\epsilon = k_2 M_*^2$ in which M_* is considered to be equal to the maximum Mach number in the domain or simply the inlet Mach number. For the subsonic (low Mach) test cases, the preconditioning parameter is simply selected to be a constant value for each test case and specific grid resolution. Computationally, k_2 found to depend on the grid resolution too [24]. Numerical experiments indicate that preconditioning the liquid phase alone is sufficient to prevent excessive numerical dissipation, an observation fully consistent with previous findings reported in [17]. This can be understood by noting that in typical two-fluid flows the liquid sound speed c_l is several orders of magnitude larger than the gas sound speed c_g, making the liquid acoustic waves the dominant source of stiffness and numerical dissipation. Preconditioning the gas phase therefore yields only a marginal benefit while introducing additional complexity into the eigenstructure of $\mathbf{P}\,\mathbf{A}$. Accordingly, in the remainder of this work we set $\beta_g = 1$, so that the preconditioner $\mathbf{P}$ acts exclusively on the liquid phase.

4. Time Stability Analysis

In the context of preconditioned single-phase equations, it is well known that preconditioning deteriorates the temporal stability of the system, reducing the allowable CFL number to values proportional to the Mach number [23, 25]. In this section the stability of the proposed scheme is investigated using the von Neumann stability analysis.

Considering only the discretized hyperbolic step given by Eq. (18), a von Neumann stability analysis can be readily performed. It is straightforward to show that the error amplification factor associated with the hyperbolic step is given by:

$$\varepsilon^* = [\mathbb{I} - \nu\,(\mathbb{i}\mathbf{A}\sin\theta + \mathbf{D}(1-\cos\theta))]\,\varepsilon^n, \tag{25}$$

where θ is the Fourier wave number, $\nu = \Delta t/\Delta x$, and $\mathbf{D}$ denotes the Roe or its preconditioned version of the diffusion matrix.

For stability, all eigenvalues of the amplification matrix must remain inside the unit circle. For the original Roe diffusion matrix, this analysis yields the classical stability limit CFL $= O(1)$. It is well known [15, 14, 26] that the preconditioned formulation imposes a more restrictive stability condition, leading to CFL $= O(M)$. Considering that, in the present work, the Mach number is of the order $O(1/c_l)$, decreasing β_l^2 dramatically reduces the stability region of the discretized equations. To illustrate this issue, Fig. 2 presents the maximum eigenvalue of Eq (25), computed numerically for a representative test case. The corresponding CFL stability limit was then determined for different values of β^2 (as it enters in the preconditioning matrix). As clearly shown in this figure, the maximum allowable CFL number is proportional to β^2, where β^2 itself is related to the Mach number, as discussed in the previous section. Consequently, reducing the value of β^2 is necessary to alleviate the excessive numerical diffusion of the five-equation model. However, this simultaneously leads to increasingly restrictive time-step limitations, requiring progressively smaller time steps. Such restrictions render the method impractical for the long-time simulations of interest in the present work.

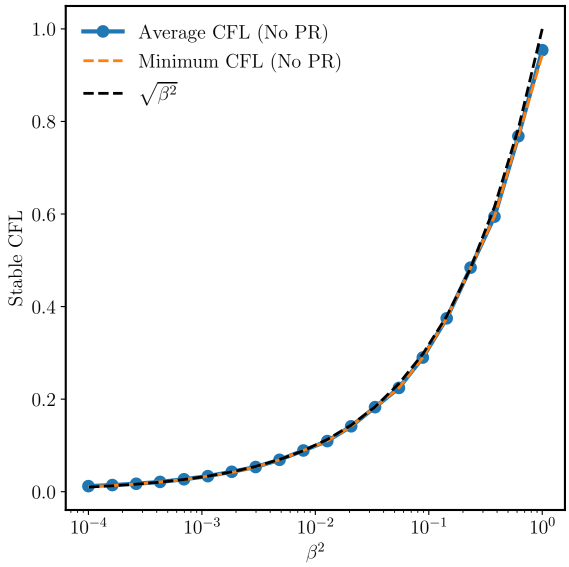

Figure 2: Maximum stable CFL number obtained from the linearized preconditioned Roe scheme without pressure relaxation. The numerical stability limit follows approximately $\mathrm{CFL}_{\max} \propto \beta_l^2$.

The above result, however, does not represent the stability of the complete algorithm because the present method contains an additional pressure-relaxation step. In this section, we show that when the hyperbolic and pressure-relaxation steps are considered together, the preconditioning does not alter the stability limit of the overall method. To demonstrate this result, we return to Eq. (15), which constitutes a nonlinear ordinary differential equation for α_g. By linearizing this equation about the state α_g^n, the following error equation can be obtained:

$$\frac{d\varepsilon_g}{dt} = -r_p \left(\frac{\rho_g c_g^2}{\alpha_g} + \frac{\rho_l c_l^2}{1-\alpha_g} \right) \varepsilon_g = \lambda \varepsilon_g. \tag{26}$$

Therefore, $\varepsilon_g^{**} = e^{\lambda \Delta t} \varepsilon_g^{*}$. In the limit $r_p \to \infty$, the amplification factor associated with the relaxation step tends to zero. Consequently, the stability of the complete scheme must be analyzed by considering the combined effect of the hyperbolic and relaxation operators. The amplification matrix of the full method is therefore obtained by multiplying the amplification factors associated with the hyperbolic and relaxation steps. It can be readily shown that the time-step restriction is not governed by all eigenvalues of the hyperbolic amplification matrix. In particular, the pressure-relaxation step selectively damps the eigenmode responsible for the restrictive stability condition introduced by the preconditioned hyperbolic operator. As a result, the problematic eigenvalue is eliminated, and the conventional CFL stability limit, CFL = $O(1)$, is recovered.

As discussed above, the relaxation step selectively affects the amplification factors of the numerical scheme. When the time step is chosen such that CFL > 1, some eigenvalues of the hyperbolic amplification matrix exceed unity, causing the hyperbolic operator to become unstable. In this situation, the relaxation step does not influence these unstable eigenmodes and, consequently, cannot restore stability. As a result, the complete operator-splitting scheme also becomes unstable.

This analysis is subject to additional limitations. As $\alpha_g \to 0$ (or $\alpha_l \to 0$), the two-fluid model degenerates into a single-phase system, and the classical preconditioning stability limit, CFL = $O(M)$, reappears. Consequently, special care must be taken in regions where one phase locally disappears, such as during slug formation or slug fronts. In such regions, the preconditioning parameter should be gradually increased toward unity, thereby recovering the original Roe formulation and avoiding the severe low-Mach-number stability restriction. Another limitation arises when the distinction between the two phases vanishes and their thermodynamic properties become nearly identical. In this limit, the term in parentheses in Eq. (26) approaches zero, thereby eliminating the influence of the pressure-relaxation parameter r_p. Consequently, the relaxation mechanism is no longer able to damp the problematic eigenmode, and the desired stability limit cannot be recovered.

5. GPU Acceleration

As discussed previously, the primary target applications of the present work involve the simulation of two-phase flows in industrial pipelines over very long time periods, often extending over several weeks of physical time. Such simulations require an extremely large number of time-integration steps over computational domains containing a large number of cells. Consequently, achieving a computationally efficient solution strategy was one of the main objectives of the present work. To this end, the proposed numerical method was implemented within a GPU (Graphics processing unit) computing framework. GPUs with their many-core architectures and high memory bandwidth, have become one of the primary platforms for high-performance scientific computing. Although the present model is one-dimensional, GPU acceleration remains highly beneficial because transient flow-assurance simulations often require long physical simulation times and consequently a very large number of time steps. Furthermore, practical engineering applications such as operational forecasting, optimization, uncertainty quantification, and digital-twin frameworks frequently require hundreds or thousands of repeated simulations, making computational efficiency a critical consideration. The numerical method described in the previous sections is particularly well suited to GPU architectures due to its explicit time-marching formulation and compact local stencil. Each cell update depends only on neighboring cells, resulting in a high degree of data parallelism and limited communication overhead. These characteristics allow efficient utilization of the massively parallel processing capabilities of modern GPUs.

In the present work, the complete numerical method is implemented on the GPU using CUDA. All solution variables are stored in GPU memory in order to minimize data transfers between the CPU and GPU. The subsequent calculations, including reconstruction, flux evaluation, source-term integration, and time advancement, are performed entirely on the GPU. Whenever data transfer to the CPU is required, for example for output operations, the memory-copy process is overlapped with kernel execution whenever possible in order to reduce communication overhead. In addition, shared memory is utilized where beneficial, and memory-access patterns are designed to maximize coalesced access to global memory. The one-dimensional structure of the solver facilitates efficient memory management and contributes to the overall computational performance. The use of GPU acceleration is motivated not only by the computational requirements of individual simulations but also by the need to perform large numbers of transient analyses within practical turnaround times. This is particularly relevant for engineering studies involving parameter sweeps, sensitivity analyses, operational decision support, and real-time flow-assurance applications. All simulations presented in Section 6 were performed on an NVIDIA Tesla V100 GPU. The high memory bandwidth and parallel-processing capabilities of this device enabled efficient execution of the proposed solver and significantly reduced the computational time required for the simulations presented in this work.

6. Numerical Results

This section assesses the performance of the proposed preconditioned five-equation model through a sequence of increasingly challenging test cases. First, a water-faucet problem is considered to verify the stability properties predicted by the theoretical analysis and to demonstrate that the pressure-relaxation step removes the severe low-Mach-number time-step restriction associated with conventional preconditioning. Next, a terrain-induced slugging benchmark in a W-shaped pipeline is used to evaluate the capability of the model to reproduce severe slugging dynamics and pressure oscillations in complex geometries. Finally, the predictive capability of the framework is examined for both Newtonian and non-Newtonian gas-liquid slug flows in inclined and vertical pipes through comparisons with experimental measurements of slug frequency and void fraction. Together, these cases provide a comprehensive assessment of the stability, accuracy, and applicability of the proposed methodology to industrial transient multiphase-flow simulations.

6.1 Water-Faucet

To illustrate the stabilizing effect of the pressure-relaxation procedure, the water-faucet test case is simulated using a fixed CFL number of 0.5 for several values of the preconditioning parameter. Figure 3 compares the numerical solutions obtained without preconditioning and with $\beta^2 = 10^{-2}$ and 10^{-4}. As discussed in section 4, the von Neumann analysis of the convective operator alone predicts that the maximum stable CFL number decreases approximately in proportion to (β^2). Consequently, values as small as ($\beta^2 = 10^{-4}$) would lead to an extremely restrictive stability limit if pressure relaxation were neglected. Nevertheless, all simulations shown in Fig. 3 remain stable at a CFL number of 0.5 and produce physically meaningful solutions. This behavior is consistent with the stability analysis of the complete algorithm, which showed that the pressure-relaxation operator introduces a strongly dissipative mode that removes the low-Mach-number time-step restriction associated with the convective update.

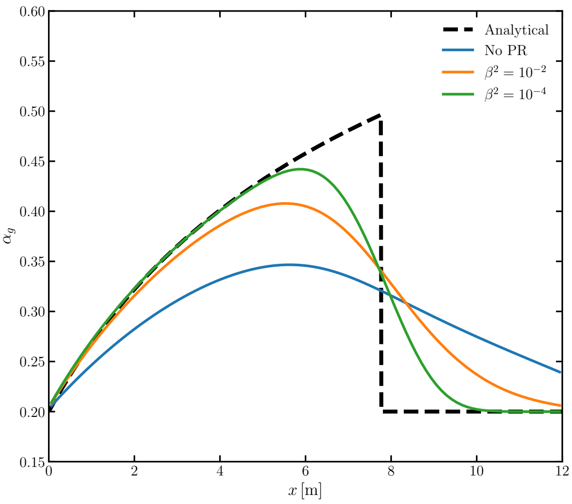

Figure 3: Gas volume fraction distribution for the water-faucet test case at $t = 0.6$ s and CFL = 0.5.

6.2 W-Shaped Pipe

The proposed model is applied to the simulation of terrain-induced slugging in a W-shaped pipeline. This benchmark represents a challenging transient gas-liquid flow problem involving liquid accumulation in low sections of the pipe, gas compression in upstream regions, slug mobilization, and periodic blowout events. Experimental measurements for this configuration were reported in [27], while a detailed numerical description of the benchmark was later presented by [28]. The computational setup follows the configuration described in [28]. The system consists of a long inclined pipe connected to a W-shaped pipeline and discharging to the atmosphere. The upstream pipe segment is used to represent the gas-liquid reservoir (tank) employed in the experiments. The inflow zone is located between this reservoir section and the first downward segment of the W-profile. Constant gas and liquid inflow rates are prescribed at this location, leading to the periodic formation, accumulation, and release of liquid slugs within the pipeline. A schematic view of the geometry is shown in Fig. 4. Further details regarding the geometric parameters and operating conditions can be found in [28]. Figure 5 compares the predicted pressure

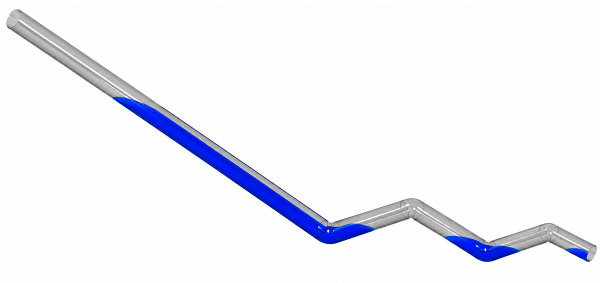

Figure 4: Schematic representation of the W-shaped pipe used for the terrain-induced slugging simulations.

histories at two observation locations with the corresponding experimental measurements from [27]. The first pressure sensor (P1) is located in the first elbow at a distance of $3.72\,m$ from the inflow zone, while the second sensor (P2) is located in the third elbow at a distance of $11.98\,m$ from the inflow zone. These locations correspond to the measurement points used in the experimental campaign and the subsequent numerical study of [28].

The current numerical predictions reproduce the principal features observed experimentally. In particular, the model captures the periodic pressure build-up, the sudden depressurization associated with slug blowout, and the overall slugging frequency. The predicted amplitudes and temporal evolution of the pressure signals are in good agreement with the measurements at both monitoring locations. Minor discrepancies are observed in some peak values and during the transient phases immediately preceding the blowout events. Such differences are expected given the highly nonlinear nature of terrain-induced slugging, where the exact timing of slug mobilization and gas breakthrough is sensitive to small perturbations and modeling assumptions.

The close agreement obtained for both pressure-monitoring locations indicates that the proposed framework captures the essential mechanisms governing terrain-induced slugging. In particular, the model accurately reproduces the cyclic sequence of liquid accumulation, gas compression, slug release, and pressure recovery that characterizes severe slugging in complex pipeline configurations.

6.3 Non-Newtonian Slug Flows

The validation cases presented so far considered Newtonian liquids. To assess the applicability of the proposed framework to non-Newtonian flows, additional simulations are performed for gas-liquid slug flows involving shear-thinning fluids. These cases provide a more stringent validation of the model since the liquid rheology directly influences the frictional pressure losses, liquid holdup, slug formation process, and slug propagation velocity.

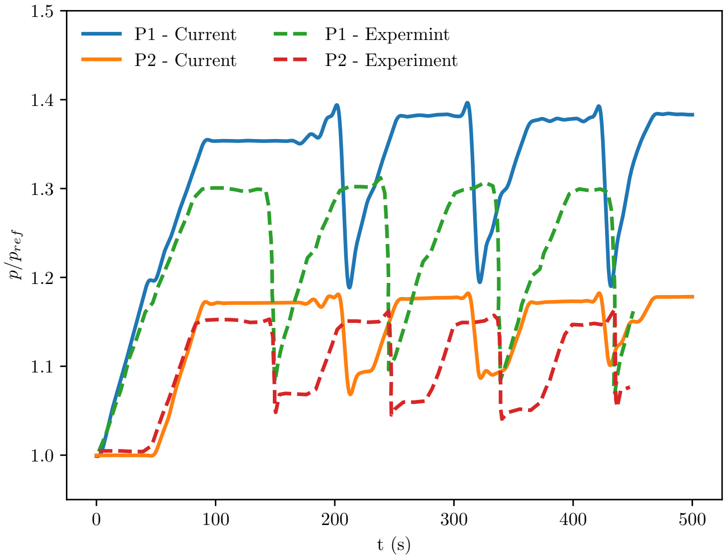

Figure 5: Comparison of predicted and experimental pressure histories at monitoring locations P1 and P2 for the W-shaped pipe test case. The numerical model accurately reproduces the periodic pressure build-up and sudden pressure drops associated with severe slugging events.

6.3.1 Air-Silicone Oil Flow in Inclined Pipes

The proposed numerical scheme is further validated against the experimental measurements of Escrig et al. [29] for intermittent air-silicone oil flow in highly inclined pipes. This benchmark is particularly suitable for assessing the ability of the model to capture the influence of gravity on slug formation and propagation. The experimental facility consists of a pipe with an inner diameter of $D = 0.067\,m$ and a total length of $L = 6\,m$, with inclination angles ranging from horizontal to vertical upward flow. Air and silicone oil are used as the gas and liquid phases, respectively, with densities $\rho_g = 1.204\,kg/m^3$ and $\rho_l = 917\,kg/m^3$, and viscosities $\mu_g = 1.74 \times 10^{-5}\,Pa.s$ and $\mu_l = 5 \times 10^{-3}\,Pa.s$. In all simulations, the wall and interfacial source terms are evaluated exclusively using the Blasius friction correlation, without any case-specific calibration or empirical tuning.

Figure 6 presents the variation of the mean slug frequency with pipe inclination for different combinations of superficial liquid and gas velocities. The numerical predictions are compared with both the experimental measurements reported by Escrig et al. [29] and the correlation proposed by Perez et al. [2]. As the inclination angle increases, the mean slug frequency also increases, reflecting the enhanced liquid accumulation and more frequent slug formation in upward inclined flows. The proposed model successfully reproduces the experimentally observed trend over the entire range of operating conditions considered. Furthermore, the numerical predictions generally exhibit better agreement with the experimental data than the correlation of Perez et al. [2], which tends to produce larger deviations for several operating conditions. These results indicate that the proposed formulation accurately captures the dominant physical mechanisms governing slug initiation and propagation in inclined pipelines. In addition to slug frequency, the cross-sectional average void fraction (VF) was evaluated at a location corresponding to 75 pipe diameters downstream of the inlet. Table 1 compares the predicted void fractions with the experimental measurements for two different sets of inlet superficial velocities. Overall, good agreement is obtained between the numerical predictions and the experimental data. With the exception of the horizontal case at the lower flow rate, the deviations remain below approximately (13%), indicating that the model accurately captures the gas-liquid phase distribution within the pipe. It is also observed that the average void fraction exhibits a weaker dependence on pipe inclination than the slug frequency. While

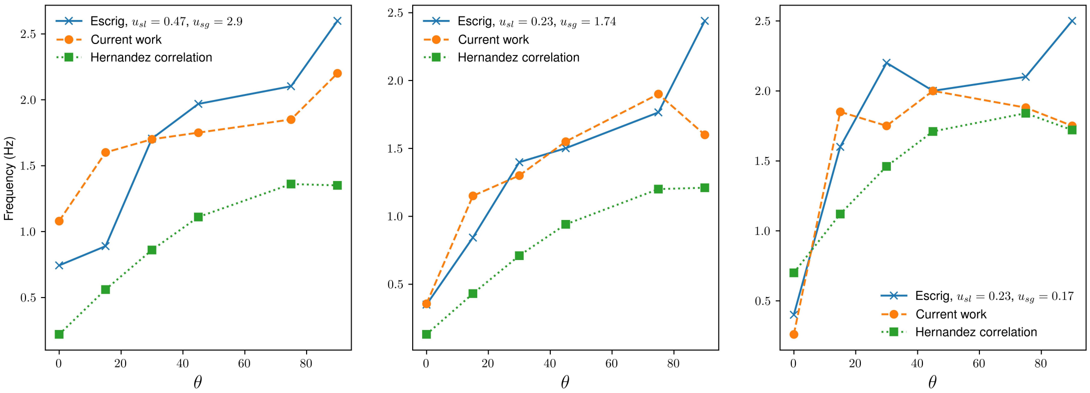

Figure 6: Mean slug frequency as a function of pipe inclination for different inlet superficial velocities. Numerical predictions are compared with the experimental measurements of Escrig et al. [29] and the correlation of Perez et al. [2].

Table 1: Comparison of the cross-sectional average void fraction (VF) with the experimental data of Escrig et al. [29].

Inclination θ	u_{sl} = 0.47 m/s, u_{sg} = 2.9 m/s			u_{sl} = 0.23 m/s, u_{sg} = 1.74 m/s		
	VF Exp.	VF Present	Error (%)	VF Exp.	VF Present	Error (%)
0	0.70	0.697	0.43	0.58	0.79	36.2
15	0.60	0.63	5.00	0.60	0.56	6.7
30	0.62	0.61	1.61	0.55	0.62	12.7
45	0.615	0.56	8.94	0.56	0.51	8.9
75	0.62	0.61	1.61	0.58	0.65	12.1
90	0.65	0.59	9.23	0.59	0.53	10.2

increasing inclination strongly affects the frequency of slug formation, its influence on the overall phase distribution is comparatively modest. This behavior is consistent with the experimental observations reported by Escrig et al. [29].

The simultaneous agreement obtained for slug frequency and void fraction demonstrates that the proposed formulation captures both the dynamic and statistical characteristics of intermittent gas-liquid flows in inclined pipes. These results further indicate that accurate predictions can be achieved without case-specific tuning of the closure relations, highlighting the robustness of the proposed approach across a wide range of inclination angles and operating conditions.

6.3.2 Air-CMC Slug Flow in Inclined Pipes

To further assess the applicability of the proposed framework to non-Newtonian flows, simulations are performed for the air-CMC experiments reported by Picchi et al. [30]. This benchmark considers intermittent gas-liquid flow involving shear-thinning liquids and therefore provides a stringent validation of the rheological extensions incorporated into the present model. The experimental facility consists of a glass pipe with a length of $L = 9\,m$ and an inner diameter of $D = 0.0228\,m$. Air is used as the gas phase, with density $\rho_g = 1.2\,kg/m^3$ and viscosity $\mu_g = 1.8 \times 10^{-5}\,Pa.s$. Three aqueous CMC solutions with different concentrations are employed as the liquid phase. Their rheological properties, represented by the power-law consistency index (K) and flow behavior index (n), are summarized in Table 2. The mean slug frequencies predicted by the present solver are compared with the experimental measurements of Picchi et al. [30] for pipe inclinations of $-5°$, $0°$, and $5°$. Table 3 summarizes the results for a representative set of operating conditions covering different gas and liquid superficial velocities as well as different CMC concentrations. As the polymer concentration increases, the liquid exhibits

Table 2: Physical properties of the CMC water solutions used in the simulations based on the experimental data of Picchi et al. [30].

Fluid type	Concentration (%)	ρ_l (kg/m^3)	K $(Pa.s^n)$	n
CMC-1	1	998.0	0.007	0.942
CMC-3	3	999.0	0.061	0.875
CMC-6	6	1002.0	0.264	0.757

stronger shear-thinning behavior, resulting in significant changes in the slugging dynamics. Despite these rheological variations, the proposed model accurately reproduces the experimentally observed slug frequencies over the entire range of conditions considered. Particularly noteworthy is the agreement obtained for the CMC-6 solution, which exhibits the strongest non-Newtonian behavior among the fluids tested.

Table 3: Comparison of slug frequencies obtained by our preconditioned first order solver and the experimental data of [30] for the two-phase flow of air-CMC water solutions with three concentrations.

Liquid phase	u_{sg} (m/s)	u_{sl} (m/s)	θ	f_s (Hz)	
				Current	[30]
CMC-1	1.22	1.32	-5	1.9	2.87
	0.61	0.26	0	0.34	0.37
	2.04	1.04	0	1.65	1.53
	1.22	1.35	5	2.0	2.14
CMC-3	1.53	0.21	0	0.61	0.61
	0.61	0.88	0	2.07	2.30
	0.92	0.13	5	1.01	0.95
CMC-6	1.22	0.82	-5	3.12	3.09
	0.92	0.15	0	0.24	0.25
	0.61	0.88	0	4.42	4.50
	1.22	0.82	5	2.84	2.91

The good agreement obtained across different CMC concentrations confirms that the rheology-dependent closure relations and the proposed numerical framework remain applicable over a broad range of shear-thinning behaviors. These results demonstrate the capability of the model to predict slug dynamics in non-Newtonian gas-liquid flows without compromising numerical robustness.

7. Conclusion

A preconditioned five-equation two-fluid model has been developed for the simulation of transient gas-liquid flows in horizontal, inclined, and vertical pipelines. The formulation combines the unconditional hyperbolicity of the five-equation model with a low-Mach-number preconditioning strategy designed to reduce the excessive numerical diffusion commonly encountered in slug-capturing simulations. A fractional-step solution procedure incorporating hyperbolic transport, pressure relaxation, and source-term integration was employed and implemented entirely on graphics processing units (GPUs) to enable efficient large-scale transient simulations.

A stability analysis of the complete operator-splitting algorithm demonstrated that, although preconditioning alone introduces the classical low-Mach-number CFL restriction, the pressure-relaxation step selectively damps the unstable mode responsible for this limitation. As a consequence, the overall numerical method preserves a stability limit of order unity while retaining the accuracy benefits of preconditioning.

The predictive capability of the proposed framework was assessed using a series of validation cases ranging from stability verification problems to severe slugging and non-Newtonian gas-liquid flows. The model successfully reproduced experimental pressure histories, slug frequencies, and void fractions over a broad range of operating conditions, pipe inclinations, and liquid rheologies. Good agreement was obtained for both Newtonian and shear-thinning liquids without the need for case-specific calibration.

The results demonstrate that the proposed methodology provides an accurate, robust, and computationally efficient framework for transient slug-flow simulations. By combining unconditional hyperbolicity, reduced numerical dissipation, favorable stability properties, and GPU acceleration, the method represents a promising tool for industrial flow-assurance applications involving long pipelines and extended physical simulation times.

Acknowledgment

The authors acknowledge the support awarded by GALP/Petrogal Brazil and ANP – Agencia Nacional de Petróleo, Gás Natural e Biocombustível.

References

[1] R. I. Issa and M. H. W. Kempf. Simulation of slug flow in horizontal and nearly horizontal pipes with the two-fluid model. *International journal of multiphase flow*, 29(1):69–95, 2003.

[2] Valente Hernandez Perez. Gas-liquid two-phase flow in inclined pipes. *University of Nottingham: Nottingham, UK*, 2007.

[3] Chengcheng Tao, Barbara G Kutchko, Eilis Rosenbaum, and Mehrdad Massoudi. A review of rheological modeling of cement slurry in oil well applications. *Energies*, 13(3):570, 2020.

[4] A.T. Bourgoyne. *Applied Drilling Engineering*. SPE textbook series. Society of Petroleum Engineers, 1986.

[5] R.P. Chhabra and J.F. Richardson. *Non-Newtonian Flow and Applied Rheology: Engineering Applications*. Elsevier Science, 2011.

[6] Marco Ferrari, Arianna Bonzanini, and Pietro Poesio. A 5-equation, transient, hyperbolic, 1-dimensional model for slug capturing in pipes. *International Journal for Numerical Methods in Fluids*, 85(6):327–362, 2017.

[7] T. N. Dinh, R. R. Nourgaliev, and T. G. Theofanous. Understanding the ill-posed two-fluid model. In *Proceedings of the 10th international topical meeting on nuclear reactor thermal-hydraulics (NURETH'03)*, 2003.

[8] M. R. Baer and J. W. Nunziato. A two-phase mixture theory for the deflagration-to-detonation transition (ddt) in reactive granular materials. *International Journal of Multiphase Flow*, 12(6):861–889, 1986.

[9] Richard Saurel and Rémi Abgrall. A multiphase godunov method for compressible multifluid and multiphase flows. *Journal of Computational Physics*, 150(2):425–467, 1999.

[10] Hervé Guillard and Angelo Murrone. On the behavior of upwind schemes in the low mach number limit: Ii. godunov type schemes. *Computers & Fluids*, 33(4):655–675, 2004.

[11] Sergiu Klainerman and Andrew Majda. Compressible and incompressible fluids. *Communications in Pure Applied Mathematics*, 35:629–651, 1982.

[12] Eli Turkel. Preconditioned methods for solving the incompressible and low speed compressible equations. *Journal of Computational Physics*, 72(2):277–298, 1987.

[13] Marica Pelanti and Keh-Ming Shyue. A roe-type scheme with low mach number preconditioning for a two-phase compressible flow model with pressure relaxation. *Bulletin of the Brazilian Mathematical Society, New Series*, 47:655–669, 2016.

[14] Philipp Birken and Andreas Meister. On low mach number preconditioning of finite volume schemes. In *PAMM: Proceedings in Applied Mathematics and Mechanics*, volume 5 (1), pages

759–760. Wiley Online Library, 2005.

[15] Marica Pelanti. Low mach number preconditioning techniques for roe-type and hllc-type methods for a two-phase compressible flow model. *Applied Mathematics and Computation*, 310:112–133, 2017.

[16] Pascal Bruel, Simon Delmas, Jonathan Jung, and Vincent Perrier. A low mach correction able to deal with low mach acoustics. *Journal of Computational Physics*, 378:723–759, 2019.

[17] Svend Tollak Munkejord. Comparison of roe-type methods for solving the two-fluid model with and without pressure relaxation. *Computers & Fluids*, 36(6):1061–1080, 2007.

[18] Randall J. LeVeque. *Finite Volume Methods for Hyperbolic Problems*. Cambridge Texts in Applied Mathematics. Cambridge University Press, 2002.

[19] Eleuterio F. Toro. *Riemann solvers and numerical methods for fluid dynamics: A practical introduction*. Springer Berlin Heidelberg, 2009.

[20] Hamidreza Anbarlooei, Daniel Onofre de Almeida Cruz, Fábio Ramos, Cecília Mageski Madeira Santos, and AP Silva Freire. On the connection between kolmogorov microscales and friction in pipe flows of viscoplastic fluids. *Physica D: Nonlinear Phenomena*, 376:69–77, 2018.

[21] M. G. Ramirez, D. O. A. Cruz, F. Nikfarjam, and H. Anbarlooei. A mechanistic model for the two-phase slug flow of the purely viscous non-newtonian liquids through pipes. *SPE Production & Operations*, 38(02):258–271, 2023.

[22] D. Guillot. Rheology of well cementing slurries. *Schlumberger Educational Services, Houston*, 1990.

[23] Hervé Guillard and Cécile Viozat. On the behaviour of upwind schemes in the low mach number limit. *Computers & fluids*, 28(1):63–86, 1999.

[24] Jean-Christophe Boniface. Rescaling of the roe scheme in low mach-number flow regions. *Journal of Computational Physics*, 328:177–199, 2017.

[25] S Venkateswaran and L Merkle. Analysis of preconditioning methods for the euler and navier-stokes equations. *Lecture series-van Kareman Institute for fluid dynamics*, 3:B1–B155, 1999.

[26] Angelo Murrone and Hervé Guillard. Behavior of upwind scheme in the low mach number limit: Iii. preconditioned dissipation for a five equation two phase model. *Computers & fluids*, 37(10):1209–1224, 2008.

[27] Vincent De Henau and GD Raithby. A study of terrain-induced slugging in two-phase flow pipelines. *International journal of multiphase flow*, 21(3):365–379, 1995.

[28] Boris I Krasnopolsky and Alexander A Lukyanov. A conservative fully implicit algorithm for predicting slug flows. *Journal of Computational Physics*, 355:597–619, 2018.

[29] Josep Escrig Escrig, Buddhika Hewakandamby, Georgios Dimitrakis, and Barry Azzopardi. Influence of inclination angle on intermittent two phase flows. In *Fluids Engineering Division Summer Meeting*, volume 50299, page V01BT28A002. American Society of Mechanical Engineers, 2016.

[30] Davide Picchi, Yuri Manerba, Sebastiano Correra, Michele Margarone, and Pietro Poesio. Gas/shear-thinning liquid flows through pipes: Modeling and experiments. *International Journal of Multiphase Flow*, 73:217–226, 2015.